IEEE Access
Multidisciplinary | Rapid Review | Open Access Journal

Received October 1, 2017, accepted February 23, 2018, date of publication March 5, 2018, date of current version April 4, 2018.

Digital Object Identifier 10.1109/ACCESS.2018.2811759

Multistage Angular Momentum Management for Space Station Attitude Control

QINGQING DANG AND LEI JIN
Beihang University, Beijing 100083, China
Corresponding author: Lei Jin (jinleibuaa@163.com)

ABSTRACT A multistage attitude control and momentum management (ACMM) control strategy is proposed for space stations. The ACMM, which includes closed-loop angular momentum feedback (CAMF) and torque equilibrium attitude (TEA) tracking, is achieved using the gravity gradient and an aerodynamic torques. The CAMF is employed as the normal flight mode, and TEA tracking is used to unload the angular momentum after attitude stabilization. Hence, the angular momentum imparted by the attitude control device does not need to be unloaded using thrusters during the entire operating phase. The system performances, especially the relationship between the environmental torques and the attitude, are analysed. The internal model principle is utilized to suppress the attitude fluctuation during the CAMF mode, and a quintic polynomial is utilized to realize TEA tracking. The pole placement algorithm, which can obtain the feedback matrix in the linear quadratic regulator (LQR) without choosing a weight matrix, is introduced to design the LQR controllers. This approach is demonstrated for a future Chinese space station, and the simulation results verified the effectiveness of the proposed control algorithm.

INDEX TERMS Attitude control and momentum management, closed-loop angular momentum feedback, torque equilibrium attitude, internal model principle, linear quadratic regulator with pole placement.

I. INTRODUCTION

As low-orbit spacecraft, space stations are exposed to spatially varying environmental torques [1]. Control moment gyros (CMGs) are usually utilized as attitude control actuators for space stations due to their ability to amplify torques [2], [3]. To minimize CMGs angular momentum and maintain a certain degree of attitude error, space stations utilize both environmental perturbations and CMGs to seek torque equilibrium attitude (TEA) during most of the time in orbit, an approach called attitude control and momentum management (ACMM) [4]. According to the different control strategies, ACMM can be divided into torque equilibrium attitude (TEA) tracking and closed-loop angular momentum feedback (CAMF).

Three-axis passive stabilization was realized using gravity gradient torques for early space stations such as Salyut 6 and Salyut 7 [5]. To desaturate the CMGs angular momentum, the Mir station let the inertia principal axis be perpendicular to the orbital plane [3]. Hattis [6] advocated momentum management for the first time officially. He reviewed the key techniques utilized on Skylab and presented the basis for space station CMGs momentum management. Kunmar [7] researched the performance of CMGs momentum management by predicting TEA using a linearized model. He focused on pitch axis control and achieved good results. Many studies on TEA employing algebra were undertaken by Sharychev [8]–[10]. He analysed different mechanical models and proposed the existence conditions for TEA. Because this type of open-loop control strategy may cause error accumulations, TEA tracking is difficult for use in long-term orbital operations.

Shain and Spector [11] developed a three-axis decouple CAMF controller architecture by first using gravity gradient torques. B. Wei then demonstrated a new momentum management controller for space stations. The gravity gradient and gyroscopic torques are utilized to seek TEA in the presence of biases and cyclic disturbances [12]. However, space stations may operate over a wide range of pitch angles, which contradicts the small-angle assumption and could produce system instabilities. To solve these problems, periodic-distance accommodating control was investigated by Warren *et al.* [13] for asymptotic momentum management, and the proposed controller employed quaternion feedback control. It was shown that a linear quadratic regulator (LQR) synthesis technique is robust over a wide range of pitch angles. Sunkel and Shieh [14] presented a multistage design

scheme for determining optimal attitude control and momentum management for the space station. However, he still assumed uncoupled roll/yaw axis and pitch axis dynamics to undertake the controller design.

Afterwards, an improved algorithm model based on a three-axis coupled model was developed by Harduvel [15]. Those studies could have been more successful if the large angle situation had been considered and if a high order matrix Q had been avoided when constructing the state feedback gain matrix by solving the Riccati equation. More recent studies have been undertaken by Zhu and Xu [4]. She converted the nonlinear system to a linear structure with state dependent coefficient matrices and needed to minimize a quadratic-like performance index. However, to trade off computation load and attitude control, the state-dependent Riccati equation was calculated online using a computationally efficient technique [16], which is difficult to be applied in practice.

However, space stations must fly under attitude stabilization for approximately 10% of the operational period during orbital rendezvous and docking [17], [18]. Obviously, this attitude stabilization mode will lead to the continuous accumulation of CMGs angular momentum. Therefore, CMGs angular momentum must be unloaded using thrusters before the space station control mode is switched from attitude stabilization to CAMF, which is costly and will impact scientific experiments, especially microgravity experiments [19], [20].

This paper presents a multistage attitude control strategy for space stations that consists of CAMF and TEA tracking. We obtained the constraint conditions by analysing the dynamic characteristics of a linearized three-axis coupled model. To design the CAMF controller, we introduced filters in the state-space equation to suppress the attitude fluctuation caused by disturbances. Before the control mode switches from attitude stabilization to CAMF mode, TEA tracking is used for the CMGs angular momentum unloading. The attitude maneuver path is planned using a quintic polynomial, and the attitude maneuver control model is obtained by transforming the nonlinear system to a linear double-integrating system. This TEA tracking design, which utilizes environmental torques to unload CMGs angular momentum, is presented for the first time. Moreover, this attitude control strategy can avoid propellant consumption and maintain the microgravity environment. For both CAMF and TEA tracking, LQR controllers are designed, and a pole placement algorithm is introduced to obtain the feedback matrix without choosing a weight matrix. We establish accurate orbit, gravity gradient and aerodynamic models to analyse system robustness.

II. SPACE STATION MODELING

A. NONLINEAR MODELS OF SPACE STATION DYNAMICS

We define three coordinate systems to describe space station motion: body frame $O_b x_b y_b z_b$, local-vertical local-horizontal (LVLH) frame $O_o x_o y_o z_o$ and inertial frame $O_i x_i y_i z_i$. In the LVLH frame, the z_o-axis points towards the earth (mass centre), the x_o-axis lies perpendicular to the z_o-axis in the orbital plane, with its positive axis in the direction of the velocity vector, and the y_o-axis is perpendicular to the orbital plane, completing the right-hand orthogonal system. The body–fixed coordinate frame and inertial frame overlaps with the LVLH frame at the initial time.

The nonlinear dynamic equation of the space station in the LVLH frame can be written as

$$\boldsymbol{I}^o\dot{\boldsymbol{\omega}}^o_{bi} + \dot{\boldsymbol{I}}^o\boldsymbol{\omega}^o_{bi} + \boldsymbol{\omega}^o_{oi} \times \boldsymbol{I}^o\boldsymbol{\omega}^o_{bi} = \boldsymbol{T}^o_c + \boldsymbol{T}^o_g + \boldsymbol{T}^o_a \tag{1}$$

where $\boldsymbol{\omega}^o_{bi}$ is the absolute angular velocity expressed in the LVLH frame, $\boldsymbol{\omega}^o_{oi}$ is the angular velocity of the LVLH frame expressed in the LVLH frame, and the right side of the equation is the total torque acting on the space station, including the output torque of CMGs $\boldsymbol{T}^o_c$, gravity gradient torque $\boldsymbol{T}^o_g$ and aerodynamic torque $\boldsymbol{T}^o_a$. $\boldsymbol{I}^o$ represents the inertia matrix expressed in the LVLH frame:

$$\boldsymbol{I}^o = C^o_b \boldsymbol{I}^b C^b_o \tag{2}$$

in which $\boldsymbol{I}^b$ is the inertia matrix of the space station expressed in the body-fixed frame:

$$\boldsymbol{I}^b = \begin{bmatrix} I_{11} & -I_{12} & -I_{13} \\ -I_{12} & I_{22} & -I_{23} \\ -I_{13} & -I_{23} & I_{33} \end{bmatrix} \tag{3}$$

The attitude of the space station is defined as the orientation of the body-fixed frame with respect to the LVLH frame and is written as $\boldsymbol{\theta} = \begin{bmatrix} \varphi & \vartheta & \psi \end{bmatrix}^{\mathrm{T}}$, where φ, ϑ and ψ are the roll, pitch and yaw angles produced through a 3-1-2 rotation sequence. The transformation matrix from the LVLH frame to the body-fixed frame is defined as

$$\boldsymbol{C}^b_o = \begin{bmatrix} c\vartheta c\psi - s\varphi s\vartheta s\psi & c\vartheta s\psi + s\varphi s\vartheta c\psi & -s\vartheta c\varphi \\ -s\psi c\varphi & c\varphi c\psi & s\varphi \\ s\vartheta c\psi + s\varphi s\psi c\vartheta & s\vartheta s\psi - s\varphi c\vartheta c\psi & c\varphi c\vartheta \end{bmatrix} \tag{4}$$

where $s \triangleq \sin$, $c \triangleq \cos$, and $C^o_b = \left[\boldsymbol{C}^b_o\right]^{\boldsymbol{T}}$. The gravity gradient torque is written as

$$\boldsymbol{T}^o_g = 3\mu/R^3 \left(\boldsymbol{\alpha}^o \times \boldsymbol{I}^o\boldsymbol{\alpha}^o\right) \tag{5}$$

where μ is the gravitational coefficient of the earth, R is the distance between the earth's mass centre and the space station's mass centre, and $\boldsymbol{\alpha}^o = \begin{bmatrix} 0 & 0 & -1 \end{bmatrix}^T$ is the unit vector from Earth's mass centre to the space station's mass centre, expressed in the LVLH frame. Given that the space station has a near-circular orbit, R can be treated as a constant, which means the orbital velocity ω_o is constant too. We then have $\mu/R^3 \approx \omega_o^2$. Substituting (2) and (3) into (5) yields

$$\boldsymbol{T}^o_g = 3\omega_o^2 \left(\boldsymbol{\alpha}^o \times \boldsymbol{C}^o_b \boldsymbol{I}^b \boldsymbol{C}^b_o \boldsymbol{\alpha}^o\right). \tag{6}$$

The aerodynamic torque described in the LVLH frame is generally estimated using the following expression:

$$\boldsymbol{T}^o_a = 0.5\rho C_D V_r^2 A_p \boldsymbol{r}^o \times \boldsymbol{V}^o \tag{7}$$

where ρ is the atmospheric density, C_D is the drag coefficient, V_r is the atmospheric velocity relative to the space station, A_p is the effective incidence area, and $\boldsymbol{r}^o$ is the vector from the centre of mass to the centre of pressure expressed in the LVLH frame, which can be written as $\boldsymbol{r}^o = \boldsymbol{C}_b^o \boldsymbol{r}^b$, where $\boldsymbol{r}^b = \begin{bmatrix} r_x^b & r_y^b & r_z^b \end{bmatrix}^T$ is the vector from the centre of mass to the centre of pressure expressed in the body frame. $\boldsymbol{V}^o$ is the unit vector of the atmospheric velocity expressed in the LVLH frame.

The attitude kinematics of the space station can be described as

$$\begin{bmatrix} \omega_{bo}^b \\ \omega_{bo}^b \\ \omega_{bo}^b \end{bmatrix} = \begin{bmatrix} -\dot{\psi} s\vartheta c\varphi + \dot{\varphi} c\vartheta \\ \dot{\psi} s\vartheta + \dot{\vartheta} \\ \dot{\psi} c\varphi c\theta + \dot{\varphi} s\vartheta \end{bmatrix} \tag{8}$$

$$\boldsymbol{\omega}_{bi}^b = \boldsymbol{\omega}_{bo}^b + \boldsymbol{C}_o^b \boldsymbol{\omega}_{oi}^o \tag{9}$$

where $\boldsymbol{\omega}_{bo}^b = \begin{bmatrix} \omega_{bo}^b & \omega_{bo}^b & \omega_{bo}^b \end{bmatrix}^T$ is the angular velocity of the body-fixed frame relative to the orbital frame with components taken in the body-fixed frame, and $\boldsymbol{\omega}_{bi}^o$ is the absolute angular velocity of the body frame relative to the inertial frame with components expressed in the LVLH frame.

The CMGs dynamic is expressed in the orbital frame as

$$\boldsymbol{T}_c^o = -\boldsymbol{\omega}_{oi}^o \times \boldsymbol{h}_c^o - \dot{\boldsymbol{h}}_c^o \tag{10}$$

where $\boldsymbol{h}_c^o$ is the angular momentum of the CMGs described in the orbital frame.

B. LINEARIZATION OF THE MODELS

To obtain the linearized model of the space station's motion, we assume that the body frame deviates from the LVLH frame by small angles. The transformation matrix $\boldsymbol{C}_o^b$ can be simplified to

$$\boldsymbol{C}_o^b \approx \boldsymbol{E} - [\boldsymbol{\theta}]^\times \tag{11}$$

where $\boldsymbol{E}$ is the unit matrix, and $[]^\times$ represents the vector cross product. The linearized expression of $\boldsymbol{I}^o$ is obtained by substituting (11) into (2) and restraining the first-order term:

$$\boldsymbol{I}^o \approx \boldsymbol{I}^o + \boldsymbol{\theta} \times \boldsymbol{I}^o - \boldsymbol{I}^o \times \boldsymbol{\theta} \tag{12}$$

The linearized equation for the gravity gradient torque can be obtained by substituting (12) into (6) and retaining the first-order terms:

$$\boldsymbol{T}_g^o = 3\omega_o^2 \begin{bmatrix} (I_{33} - I_{22}) & -I_{12} & I_{13} \\ -I_{12} & (I_{33} - I_{11}) & I_{23} \\ 0 & 0 & 0 \end{bmatrix} \begin{bmatrix} \varphi \\ \vartheta \\ \psi \end{bmatrix} + 3\omega_o^2 \begin{bmatrix} I_{23} \\ -I_{13} \\ 0 \end{bmatrix} \tag{13}$$

The gravity gradient torque can be divided into attitude-dependent and attitude-independent terms, and the attitude-dependent term can be used for momentum management.

To obtain the linearized attitude related terms for the aerodynamic torque, we assume that V_r is a constant and that $\boldsymbol{V}^o = \begin{bmatrix} -1 & 0 & 0 \end{bmatrix}^T$ is a constant vector, and the atmospheric density is assumed to change with time in sinusoidally. When the space station is flying in an earth-oriented flight attitude, the solar arrays should track the sun. The effective incidence area A_p in (7) can be generally divided into an average part and cyclic components. Based on the above assumptions, the aerodynamic torque can be divided into the attitude related term and $\boldsymbol{T}_d^o$:

$$\boldsymbol{T}_a^o \approx \begin{bmatrix} 0 & 0 & 0 \\ -t_y & t_x & 0 \\ -t_z & 0 & t_x \end{bmatrix} \begin{bmatrix} \varphi \\ \vartheta \\ \psi \end{bmatrix} + \boldsymbol{T}_d^o \tag{14}$$

where

$$\begin{cases} t_x = 0.5 C_D V_r^2 r_x^b \left(\omega_o / 2\pi\right) \displaystyle\int_0^{2\pi/\omega_o} \rho A_p dt \\ t_y = 0.5 C_D V_r^2 r_y^b \left(\omega_o / 2\pi\right) \displaystyle\int_0^{2\pi/\omega_o} \rho A_p dt \\ t_z = 0.5 C_D V_r^2 r_z^b \left(\omega_o / 2\pi\right) \displaystyle\int_0^{2\pi/\omega_o} \rho A_p dt \end{cases} \tag{15}$$

The angular momentum of the space station in the orbital frame $\boldsymbol{H}_s^o$ can be described as

$$\boldsymbol{H}_s^o = \boldsymbol{I}^o \boldsymbol{\omega}_{bi}^o \tag{16}$$

Upon further analysis, we find that the angular momentum of the space station can be divided into a time-varying component and a constant component (gyroscopic coupling item):

$$\boldsymbol{H}_s^o = \bar{\boldsymbol{H}}_s^o + \Delta \boldsymbol{H}_s^o \tag{17}$$

To make $\Delta \boldsymbol{H}_s^o = \boldsymbol{0}$ when the LVLH frame overlaps the body frame, the constant component is defined as $\bar{\boldsymbol{H}}_s^o = \boldsymbol{I}^b \boldsymbol{\omega}_{oi}^o$. Note that the inertia matrix is expressed in the body frame and that $\boldsymbol{\omega}_{oi}^o$ is described in the orbital frame. By combining (13), (14), (16) and (17), the dynamics of the space station described in (1) can be rearranged to

$$\Delta \dot{\boldsymbol{H}}_s^o = -\boldsymbol{\omega}_{oi}^o \times \Delta \boldsymbol{H}_s^o + \boldsymbol{T}_{ec}^o + \boldsymbol{T}_c^o + \boldsymbol{T}_d^o - \boldsymbol{\omega}_{oi}^o \times \bar{\boldsymbol{H}}_s^o + 3\omega_o^2 \begin{bmatrix} I_{23} & -I_{13} & 0 \end{bmatrix}^{\mathrm{T}} \tag{18}$$

where

$$\boldsymbol{T}_{ec}^o = \begin{bmatrix} 3\omega_o^2 (I_{33} - I_{22}) & -3\omega_o^2 I_{12} & 3\omega_o^2 I_{13} \\ -t_y - 3\omega_o^2 I_{12} & 3\omega_o^2 (I_{33} - I_{11}) + t_x & 3\omega_o^2 I_{23} \\ -t_z & 0 & t_x \end{bmatrix} \times \begin{bmatrix} \varphi \\ \vartheta \\ \psi \end{bmatrix} \tag{19}$$

The attitude related environment control torques $\boldsymbol{T}_{ec}^o$ in the above equation are obtained from (13) and (14). Moreover, $\boldsymbol{T}_{ec}^o$ is very significant to momentum management because it determines which environmental torques will be utilized for attitude movement. Obviously, no gravity gradient torque related to attitude can be produced in the yaw axis for momentum management, and the aerodynamic torque is much smaller than the gravity gradient torque. Therefore, it is difficult for the space station to offset the disturbance torque in the yaw direction. To solve this problem, the roll angle will be used to offset the disturbance torque in the yaw

axis. Additional details will be discussed in the next section. To obtain the linearized attitude kinematics, we assume that

$$\boldsymbol{C}_b^o \boldsymbol{\omega}_{bo}^b \approx \dot{\boldsymbol{\theta}} \tag{20}$$

$$\left(\boldsymbol{I}^o\right)^{-1} = \left(\boldsymbol{I}^b\right)^{-1} + \boldsymbol{\theta} \times \left(\boldsymbol{I}^b\right)^{-1} - \left(\boldsymbol{I}^b\right)^{-1} \times \boldsymbol{\theta} \tag{21}$$

The attitude kinematics can be linearized by substituting (9), (17), (20), and (21) into (16) and restraining first-order term:

$$\dot{\boldsymbol{\theta}} = \left[\left(\boldsymbol{I}^b\right)^{-1} \times \bar{\boldsymbol{H}}_s^o - [\boldsymbol{\theta}]^{\times}\right]\boldsymbol{\theta} + \left(\boldsymbol{I}^b\right)^{-1} \Delta \boldsymbol{H}_s^o \tag{22}$$

III. DYNAMIC CHARACTERISTIC ANALYSIS

A. ATTITUDE CONTROL AND MOMENTUM MANAGEMENT ANALYSIS

Before analysing the ACMM model, we should determine which form of disturbance causes CMGs momentum accumulation and which form of attitude manoeuvre could avoid CMGs saturation. To obtain a constant disturbance in the inertial frame, the aerodynamic item unrelated to attitude in (14) is expressed as

$$\boldsymbol{T}_d^o = \begin{bmatrix} T_{x0}^o \\ T_{y0}^o \\ T_{z0}^o \end{bmatrix} + \begin{bmatrix} a\sin(\omega_o t) + b\cos(\omega_o t) \\ T_{y1}^o \sin(\omega_o t + \varphi_y) \\ c\sin(\omega_o t) + d\cos(\omega_o t) \end{bmatrix} + \begin{bmatrix} T_{x2}^o \sin(2\omega_o t + \varphi_{2x}) \\ T_{y2}^o \sin(2\omega_o t + \varphi_{2y}) \\ T_{z2}^o \sin(2\omega_o t + \varphi_{2z}) \end{bmatrix} \tag{23}$$

where $\boldsymbol{T}_{d0}^o = \begin{bmatrix} T_{x0}^o & T_{y0}^o & T_{z0}^o \end{bmatrix}^{\mathrm{T}}$ is constant in the orbital frame, a, b, c, d, and T_{y1}^o are constant coefficients, φ_y is the phase of the pitch at frequency ω_o, $\boldsymbol{T}_{d2}^o = \begin{bmatrix} T_{x2}^o & T_{y2}^o & T_{z2}^o \end{bmatrix}^T$ is the coefficient of $2\omega_o$, and $\boldsymbol{\varphi}_2 = \begin{bmatrix} \varphi_{2x} & \varphi_{2y} & \varphi_{2z} \end{bmatrix}^T$ is the phase of $2\omega_o$. Assuming that the gravity gradient torque and the aerodynamic torque are fully absorbed by CMGs, we have

$$\boldsymbol{T}_g^i + \boldsymbol{T}_a^i = -\boldsymbol{T}_c^i \tag{24}$$

The angular momentum of CMGs in the inertial frame can be obtained from (10):

$$\boldsymbol{T}_c^i = -\boldsymbol{C}_o^i \boldsymbol{\omega}_{oi}^o \times \boldsymbol{h}_c^o - \boldsymbol{C}_o^i \dot{\boldsymbol{h}}_c^o \tag{25}$$

Obviously, the constant disturbance expressed in the inertial frame could cause CMGs angular momentum accumulation. Namely, the constant disturbance expressed in the inertial frame should be offset by extra torques such as the gravity gradient torque and aerodynamic torque. The pitch axis in the LVLH frame can be regarded as an inertial axis, and the roll /yaw axes are rotating around the pitch axis at the orbital frequency. We divide the disturbance into two components: that perpendicular to the orbital plane part and the component in the orbital plane. Because a disturbance in pitch can be offset by a constant bias in the pitch axis according to (19), we assume that $\Delta \dot{\boldsymbol{H}}_s^o(2) = 0$ in (18), and hence the dynamics of the space station in the pitch axis can be rewritten as

$$\left(-t_y - 3\omega_o^2 I_{12}\right)\varphi + \left[3\omega_o^2 (I_{33} - I_{11}) + t_x\right]\vartheta + 3\omega_o^2 I_{23}\psi + T_{dy}^o = 3\omega_o^2 I_{13} \tag{26}$$

Ignoring the impact of the coupling effect between roll/yaw and pitch, we decouple the pitch axis from the yaw/roll axes. The TEA in pitch can be estimated using the following equation:

$$\theta_{0y} = \left(T_{y0}^o - 3\omega_o^2 I_{13}\right) / \left[3\omega_o^2 (I_{11} - I_{33}) - t_x\right] \tag{27}$$

The following analysis will show that the attitude error in yaw can be held to zero by the roll axis undergoing a sinusoidal motion at the orbital frequency. The estimated error in pitch caused by the decoupling is very small.

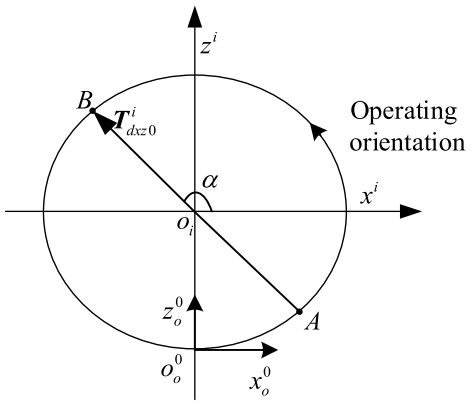

FIGURE 1. Constant disturbance in the orbital plane.

To make the explanation more visual, the constant disturbance in the orbital plane is illustrated in Fig. 1. The vector $\overrightarrow{AB}$ represents the orientation of the constant component of the disturbance torque $\boldsymbol{T}_d^i$ in the orbital plane, and α is the angle between $\boldsymbol{T}_{dxz0}^i$ and ox^i. The inertial and LVLH frames overlap at the initial time. The angle between x_o and x_i is $\omega_o t$ at time t, and the transformation matrix from the LVLH frame to the inertial frame is defined as

$$C_o^i = \begin{bmatrix} \cos\omega_o t & 0 & -\sin\omega_o t \\ 0 & 1 & 0 \\ \sin\omega_o t & 0 & \cos\omega_o t \end{bmatrix} \tag{28}$$

To obtain the constant component of $\boldsymbol{T}_d^i$ in the inertial frame, $\boldsymbol{T}_{d0}^i = \begin{bmatrix} T_{x0}^i & T_{y0}^i & T_{x0}^i \end{bmatrix}^T$, we need to express the orbital frequency component of $\boldsymbol{T}_d^0$ in the inertial frame and retain the constant term:

$$\boldsymbol{T}_{d0}^i = \begin{cases} 0.5(b-c) \\ T_{y0}^o \\ 0.5(a+d) \end{cases} \tag{29}$$

This means $\left|\boldsymbol{T}_{dxz0}^i\right| = 0.5\sqrt{(b-c)^2 + (a+d)^2}$ is determined by the phases of $\boldsymbol{T}_d^o$ at the orbital frequency, and

$$\alpha = \arccos\left[0.5(b-c) / \left|\boldsymbol{T}_{dxz0}^i\right|\right] \tag{30}$$

The disturbance in the orbital plane shown in Fig. 1 must be offset by the roll/yaw motion. However, the aerodynamic torque is very small, the yaw motion can produce very limited torques according to (19), and we utilize the roll axis motion to produce a control torque in the orbital plane and keep the attitude stable in yaw. When the space station operates in the orbital arc $\widehat{AB}$, the roll should produce a control torque in the opposite direction of the roll axis to offset the disturbance in the orbital plane. Similarly, when the space station is operating on the orbital arc $\widehat{BA}$, the roll should produce a control torque in the positive direction of $o_o x_o$ to offset the disturbance in the orbital plane. In this case, the roll axis will undergo a sinusoidal motion at the orbital frequency.

For example, if $(I_{33} - I_{22}) > 0$, and $\varphi < 0$, the roll axis will produce a torque in the minus $o_o x_o$ on the orbital arc AB, and the component of the environmental control torque $\boldsymbol{T}_{ec}^{o} = \left[T_{ecx}^{o} \;\; T_{ecy}^{o} \;\; T_{ecz}^{o} \right]^{T}$ in (19) in the roll axis at any time used to offset the disturbance is

$$T_{ecx}^{o} = 3\omega_o^2 \left(I_{33} - I_{22}\right) \varphi \tag{31}$$

where

$$\varphi = -k_\varphi \cos\left(\omega_o t - \alpha\right) sign\left(I_{33} - I_{22}\right) \tag{32}$$

$k_\varphi \geq 0$, and sign(.) is the signum function.

Similarly, the roll axis will manoeuvre to $\varphi > 0$ on the orbital arc $\widehat{BA}$, and therefore no angular momentum will be accumulated in the vertical orientation of $\boldsymbol{T}_{dxz0}^{i}$ by symmetry. The absolute in-plane value of $\boldsymbol{T}_{d}^{o}$ is

$$\left| \boldsymbol{T}_{dxz0}^{i} \right| = \left| \left(\omega_o / 2\pi\right) \int_0^{2\pi/\omega_o} T_{ecx}^{o} \cos\left(\omega_o t - \alpha\right) dt \right| \tag{33}$$

k_φ is solved using (31) and (33), and upon substitution into (32),

$$\varphi = -\left(\left| \boldsymbol{T}_{dxz0}^{i} \right| / \left| 1.5\omega_o^2 \left(I_{33} - I_{22}\right) \right| \right) \times \cos\left(\omega_o t - \alpha\right) sign\left(I_{33} - I_{22}\right) \tag{34}$$

Based on the above analysis, we find that the pitch angle retains a constant bias when the roll performs circular motion at the orbital frequency. All of the disturbances, with the exception of the constant component in the inertial frame, will be absorbed by CMGs. To reduce the error between the actual system and the nominal system, the attitude angles should be as small as possible, and the correlation coefficient of the environmental torques should therefore meet the constraint conditions

$$\begin{cases} \left| 3\omega_o^2 (I_{11} - I_{33}) - t_x \right| \gg 0 \\ \left| 3\omega_o^2 \left(I_{33} - I_{22}\right) \right| \gg 0 \end{cases} \tag{35}$$

B. ATTITUDE PATH PLANNING

The space station needs to maintain stability during rendezvous and docking, which will cause an accumulation of angular momentum. If we switch the control mode to CAMF without unloading the angular momentum, the system may shake or even become unstable. We use TEA tracking to unload the angular momentum accumulation caused by attitude stabilization, and TEA tracking is achieved by attitude path planning.

As analysed above, the angular momentum of CMGs can be unloaded by an attitude manoeuvre in the roll and pitch axes, and the attitude path can therefore be defined as $\boldsymbol{\theta}_d = \left[\varphi_d \;\; \vartheta_d \;\; 0 \right]^{\mathrm{T}}$. The attitude path, whether in the roll axis or pitch axis, can be divided into three parts: manoeuvring to desired attitude, attitude maintaining and manoeuvring to zero-attitude. The attitude manoeuvre process is shown in Fig. 2.

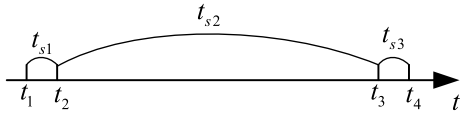

FIGURE 2. Time allocation schematic of attitude manoeuvre.

We utilize a quintic polynomial to plan the attitude path, which ensures angular and angular velocity continuity. For the pitch angle,

$$\vartheta_d = \begin{cases} k_{y1} \left[(t - t_1)^5 + a_{y1} (t - t_1)^4 + b_{y1} (t - t_1)^3 \right] \\ \qquad t_1 < t < t_2 \\ \vartheta_1 \quad t_2 < t < t_3 \\ k_{y2} \left[(t - t_3)^5 + a_{y2} (t - t_3)^4 + b_{y2} (t - t_3)^3 \right] + \vartheta_1 \\ \qquad t_3 < t < t_4 \end{cases} \tag{36}$$

where

$$\begin{cases} k_{y1} = 6\vartheta_1 / t_{s1}^5 \\ a_{y1} = -(5/2)\, t_{s1} \\ b_{y1} = (5/3)\, t_{s1}^2, \end{cases} \qquad \begin{cases} k_{y2} = -6\vartheta_1 / t_{s3}^5 \\ a_{y2} = -(5/2)\, t_{s3} \\ b_{y2} = (5/3)\, t_{s3}^2 \end{cases}$$

ϑ_1 is the steady state attitude, which can be estimated using the initial CMGs angular momentum and attitude related coefficient:

$$\vartheta_1 = \left[\omega_o h_{ucy}^{o} / 2\pi n + T_{dy}^{b} \right] / \left[3\omega_o^2 (I_{11} - I_{33}) - t_x \right] \tag{37}$$

where $n = \mathrm{t_{s2}}\omega_o / 2\pi$ is the number of orbital periods used to unload the CMGs angular momentum, which can be set based on the situation.

$$\varphi_d = \begin{cases} k_{x1} \left[(t - t_1)^5 + a_{x1} (t - t_1)^4 + b_{x1} (t - t_1)^3 \right] \\ -k_x \cos\left(\omega_0 t - \alpha\right) sign\left(I_{33} - I_{22}\right) \\ k_{x2} \left[(t - t_3)^5 + a_{x2} (t - t_3)^4 + b_{x2} (t - t_3)^3 \right. \\ \quad \left. + e_{x2} (t - t_3) \right] + \varphi_2 \\ \qquad t_1 < t < t_2 \\ \qquad t_2 < t < t_3 \\ \qquad t_3 < t < t_4 \end{cases} \tag{38}$$

where

$$\begin{cases} k_{x1} = 0.01 / t_{s1}^5 \\ a_{x1} = (-300\varphi_1 + 100 t_{s1} \dot{\varphi}_1 - 2)\, t_{s1} \\ b_{x1} = (1 + 400\varphi_1 - 100 t_{s1} \dot{\varphi}_1)\, t_{s1}^2, \end{cases}$$

$$\begin{cases} k_{x2} = 0.01/t_{s3}^5 \\ a_{x2} = (300\varphi_2 + 200t_{s3}\dot{\varphi}_2 - 2)\, t_{s3} \\ b_{x2} = (1 - 400\varphi_2 - 300t_{s3}\dot{\varphi}_2)\, t_{s3}^2 \\ e_{x2} = 100t_{s3}^5\dot{\varphi}_2 \end{cases}$$

$$\begin{cases} \varphi_1 = -k_x \cos(\omega_0 t_2 - \alpha)\, sign\,(I_{33} - I_{22}) \\ \varphi_2 = -k_x \cos(\omega_0 t_3 - \alpha)\, sign\,(I_{33} - I_{22}) \end{cases} \quad (39)$$

k_x is the maximum steady state attitude, which can be estimated using the initial CMGs angular momentum and attitude related coefficient:

$$k_x = \left|\omega_o \boldsymbol{h}_{ucxz}^i / (2\pi n) + \boldsymbol{T}_{xzd0}^i\right| / \left[1.5\omega_o^2 (I_{33} - I_{22})\right] \quad (40)$$

Because the angular momentum of CMGs in the orbital plane, $\boldsymbol{h}_{ucxz}^i$, is generated using the constant disturbance in the orbital plane, $\boldsymbol{T}_{xzd0}^i$, it is reasonable to assume that $\boldsymbol{h}_{ucxz}^i$ is parallel to $\boldsymbol{T}_{xzd0}^i$, which means the phase angle α in (39) is the same as the phase angle shown in Fig. 1.

NOTE 1: The attitude path planned in this part is based on the dynamic characteristics and CMGs angular momentum that needs to be unloaded. The effect of unloading depends on the accuracies of the models, especially the disturbance model, and it is therefore difficult to unload the CMGs angular momentum to precisely zero.

IV. CONTROLLER DESIGN

A. TORQUE EQUILIBRIUM ATTITUDE TRACKING

Because of the large angles in attitude manoeuvres, the linearized model cannot be used to design the TEA tracking controller. The nonlinear dynamic model of (1) is expressed in the body frame:

$$\boldsymbol{I}^b\dot{\boldsymbol{\omega}}_{bi}^b + \dot{\boldsymbol{I}}^b\boldsymbol{\omega}_{bi}^b + \boldsymbol{\omega}_{bi}^b \times \boldsymbol{I}^b\boldsymbol{\omega}_{bi}^b = \boldsymbol{T}_c^b + \boldsymbol{T}_g^b + \boldsymbol{T}_a^b \quad (41)$$

Taking the derivative of (9),

$$\dot{\boldsymbol{\omega}}_{bi}^b = \Phi\ddot{\boldsymbol{\theta}} + \boldsymbol{f}_\vartheta \quad (42)$$

where

$$\Phi = \begin{bmatrix} c\vartheta & 0 & -c\varphi s\vartheta \\ 0 & 1 & s\varphi \\ s\vartheta & 0 & c\varphi c\vartheta \end{bmatrix}.$$

$\boldsymbol{f}_\vartheta$ is a function that is related to the angles and angular velocity (43), as shown at the bottom of this page.

By substituting (42) into (41), the double integral model is obtained:

$$\ddot{\boldsymbol{\theta}} = \boldsymbol{U} \quad (44)$$

where

$$\boldsymbol{U} = \left(\boldsymbol{I}^b\Phi\right)^{-1}\left[\boldsymbol{T}_c^b + \boldsymbol{T}_g^b + \boldsymbol{T}_a^b - \boldsymbol{\omega}_{oi}^b \times \boldsymbol{I}^b\boldsymbol{\omega}_{bi}^b - \boldsymbol{I}^b\boldsymbol{f}_\vartheta\right] \quad (45)$$

To obtain the track error, define

$$\Delta\boldsymbol{\theta} = \boldsymbol{\theta}_d - \boldsymbol{\theta} \quad (46)$$

Taking the derivative of (46) twice and substituting (44) into the result yields

$$\Delta\ddot{\boldsymbol{\theta}} = \ddot{\boldsymbol{\theta}}_d - \boldsymbol{U} \quad (47)$$

Choosing the state values $\boldsymbol{x} = \left[\,\Delta\boldsymbol{\theta}\ \ \Delta\dot{\boldsymbol{\theta}}\,\right]^T$ and combining (44), (46) and (47) yields

$$\dot{\boldsymbol{x}}_2 = \begin{bmatrix} \boldsymbol{0} & \boldsymbol{E} \\ \boldsymbol{0} & \boldsymbol{0} \end{bmatrix}\boldsymbol{x}_2 + \begin{bmatrix} \boldsymbol{0} \\ \boldsymbol{E} \end{bmatrix}\boldsymbol{u}_2 \quad (48)$$

where $\boldsymbol{u}_2 = \ddot{\boldsymbol{\theta}}_d - \boldsymbol{U}$, and

$$\boldsymbol{u}_2 = -\boldsymbol{K}_2\boldsymbol{x}_2 \quad (49)$$

We can obtain the CMGs control torque from (45):

$$\boldsymbol{T}_c^b = \left(\boldsymbol{I}^b\Phi\right)\boldsymbol{U} - \boldsymbol{T}_g^b - \boldsymbol{T}_a^b + \boldsymbol{\omega}_{oi}^b \times \boldsymbol{I}^b\boldsymbol{\omega} + \boldsymbol{I}^b\boldsymbol{f}_\vartheta.$$

Feedback matrix $\boldsymbol{K}_2$ can be obtained using the linear quadratic regulator with the eigenvalue placement algorithm presented in section IV, part C.

B. CLOSED-LOOP ANGULAR MOMENTUM FEEDBACK

The attitude error and CMGs angular momentum should be constrained simultaneously in CAMF. $\Delta\boldsymbol{H}_s^o$ contains the information about the angular velocity, hence the CAMF model is completely described by (10) (18) and (22). We choose the augment state variables as $\boldsymbol{x} = \left[\,\Delta\boldsymbol{H}_s^o\ \ \boldsymbol{\theta}\ \ \boldsymbol{h}_c^o\,\right]^T$ and rewrite these equations into the form of the state space equation:

$$\begin{cases} \dot{\boldsymbol{x}}_1 = \boldsymbol{A}_1\boldsymbol{x}_1 + \boldsymbol{B}_1\boldsymbol{T}_c^o + \boldsymbol{B}_w\boldsymbol{w} \\ \boldsymbol{u}_1 = -\boldsymbol{K}_1\boldsymbol{x}_1 \end{cases} \quad (50)$$

where

$$\boldsymbol{A}_1 = \begin{bmatrix} -\left[\boldsymbol{\omega}_{oi}^o\right]^\times & \boldsymbol{A}_{T\theta} & \boldsymbol{0} \\ \left(\boldsymbol{I}^b\right)^{-1} & \boldsymbol{A}_{\theta\theta} & \boldsymbol{0} \\ \boldsymbol{0} & \boldsymbol{0} & -\left[\boldsymbol{\omega}_{oi}^o\right]^\times \end{bmatrix},$$

$$\boldsymbol{B}_1 = \left[\boldsymbol{E}\quad \boldsymbol{0}\quad -\boldsymbol{E}\right]^T,\quad \boldsymbol{B}_w = \left[\boldsymbol{E}\quad \boldsymbol{0}\quad \boldsymbol{0}\right]^T, \text{ and}$$

$$\boldsymbol{w} = \boldsymbol{T}_d^o + \bar{\boldsymbol{H}}_s^o + 3\omega_o^2\begin{bmatrix} I_{23} \\ -I_{13} \\ 0 \end{bmatrix},$$

$$\boldsymbol{A}_{\theta\theta} = \left[\left(\boldsymbol{I}^b\right)^{-1} \times \bar{\boldsymbol{H}}_s^o - [\boldsymbol{\theta}]^\times\right].$$

To reduce the disadvantageous effects of disturbances on the attitude and allow the space station to perform the desired motion mentioned, we suppress the disturbance using the internal model principle [21]. The internal model applies to

$$\boldsymbol{f}_\vartheta = \begin{bmatrix} -\dot{\varphi}\dot{\vartheta}s\vartheta - \dot{\vartheta}\dot{\psi}c\varphi c\vartheta + \dot{\varphi}\dot{\psi}s\varphi s\vartheta \\ \dot{\varphi}\dot{\psi}c\varphi \\ \dot{\varphi}\dot{\vartheta}c\vartheta - \dot{\varphi}\dot{\psi}s\varphi c\vartheta - \dot{\vartheta}\dot{\psi}c\varphi s\vartheta \end{bmatrix} + \omega_o \times \begin{bmatrix} -\dot{\varphi}c\varphi s\vartheta c\psi + \dot{\vartheta}\,(s\vartheta s\psi - s\varphi c\vartheta c\psi) + \dot{\psi}\,(s\varphi s\vartheta s\psi - c\vartheta c\psi) \\ \dot{\psi}s\psi c\varphi + \dot{\varphi}s\varphi c\psi \\ \dot{\varphi}c\varphi c\vartheta c\psi - \dot{\vartheta}\,(s\varphi s\vartheta c\psi + c\vartheta s\psi) - \dot{\psi}\,(s\varphi c\vartheta s\psi + s\vartheta c\psi) \end{bmatrix} \quad (43)$$

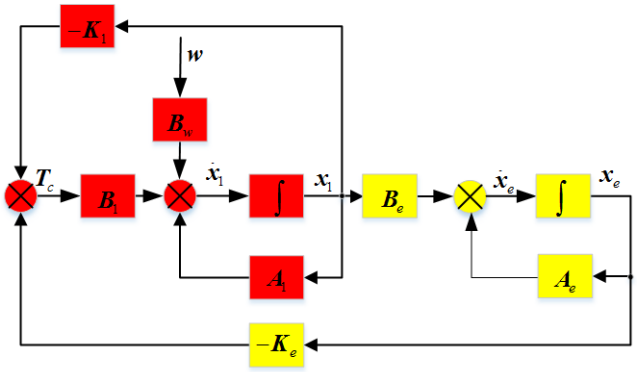

FIGURE 3. System structure of CAMF.

linear or weakly nonlinear systems. The necessary condition for ensuring the stability of the system shown in Fig. 3 is that the basic system (the red part in Fig. 3; (50)) is stable [22]. Fortunately, we have analysed the controllability of the basic system from the characteristics of ACMM and have obtained the following theorem.

Theorem: The system described in (50) is controllable if and only if (35) is satisfied. This theorem can be easily proven using the Popov–Eleventh–Hautus Criterion [23].

The disturbance mainly includes the constant term, the period term at a single frequency and high frequency terms. According to the internal model principle, it is necessary to model the disturbance for control. The compensator (the yellow part shown in Fig. 3 is utilized to suppress the influence of high frequency disturbances on the attitude angle and to avoid the accumulation of CMGs angular momentum caused by constant disturbances:

$$\begin{cases} \dot{\boldsymbol{x}}_e = \boldsymbol{A}_e \boldsymbol{x}_e + \boldsymbol{B}_e \boldsymbol{x} \\ \boldsymbol{u}_e = -\boldsymbol{K}_e \boldsymbol{x}_e \end{cases} \tag{51}$$

where

$$\boldsymbol{x}_e = \begin{bmatrix} f0 & f1_1 & f1_2 & f2_1 & f2_2 & f3_1 & f3_2 \end{bmatrix}^T,$$

$$\boldsymbol{A}_e = \begin{bmatrix} \boldsymbol{0} & \boldsymbol{0} & \boldsymbol{0} & \boldsymbol{0} & \boldsymbol{0} & \boldsymbol{0} & \boldsymbol{0} \\ \boldsymbol{0} & \boldsymbol{0} & \boldsymbol{E} & \boldsymbol{0} & \boldsymbol{0} & \boldsymbol{0} & \boldsymbol{0} \\ \boldsymbol{0} & -\omega_o^2 \boldsymbol{E} & \boldsymbol{0} & \boldsymbol{0} & \boldsymbol{0} & \boldsymbol{0} & \boldsymbol{0} \\ \boldsymbol{0} & \boldsymbol{0} & \boldsymbol{0} & \boldsymbol{0} & \boldsymbol{E} & \boldsymbol{0} & \boldsymbol{0} \\ \boldsymbol{0} & \boldsymbol{0} & \boldsymbol{0} & -\lambda_1^2 \omega_o^2 \boldsymbol{E} & \boldsymbol{0} & \boldsymbol{0} & \boldsymbol{0} \\ \boldsymbol{0} & \boldsymbol{0} & \boldsymbol{0} & \boldsymbol{0} & \boldsymbol{0} & \boldsymbol{0} & \boldsymbol{E} \\ \boldsymbol{0} & \boldsymbol{0} & \boldsymbol{0} & \boldsymbol{0} & \boldsymbol{0} & -\lambda_2^2 \omega_o^2 \boldsymbol{E} & \boldsymbol{0} \end{bmatrix},$$

and

$$\boldsymbol{B}_e = \begin{bmatrix} \boldsymbol{0} & \boldsymbol{A}_{0\theta} & \boldsymbol{A}_{0h} \\ \boldsymbol{0} & \boldsymbol{0} & \boldsymbol{0} \\ \boldsymbol{0} & \boldsymbol{A}_{1\theta} & \boldsymbol{A}_{1h} \\ \boldsymbol{0} & \boldsymbol{0} & \boldsymbol{0} \\ \boldsymbol{0} & \boldsymbol{E} & \boldsymbol{0} \\ \boldsymbol{0} & \boldsymbol{0} & \boldsymbol{0} \\ \boldsymbol{0} & \boldsymbol{E} & \boldsymbol{0} \end{bmatrix}.$$

λ_1 and λ_2 are coefficients of ω_o, which means disturbances with frequencies ω_o, $\lambda_1\omega_o$, and $\lambda_2\omega_o$ are suppressed by the controller. To ensure the system is controllable, λ_1 and λ_2 should meet the constraint $\lambda_2 > \lambda_1 > 1$. Based on the analysis in section III, the pitch must contain bias, and the moving mode of the row is chosen as a sinusoidal movement at the orbital frequency to offset the torques that could cause CMGs angular momentum accumulation in a steady state. To achieve this effect, filter matrices are defined as follows:

$$\boldsymbol{A}_{0\theta} = \begin{bmatrix} 1 & 0 & 0 \\ 0 & 0 & 0 \\ 0 & 0 & 1 \end{bmatrix}, \quad \boldsymbol{A}_{0h} = \begin{bmatrix} 0 & 0 & 0 \\ 0 & 1 & 0 \\ 0 & 0 & 0 \end{bmatrix},$$

$$\boldsymbol{A}_{1\theta} = \begin{bmatrix} 0 & 0 & 0 \\ 0 & 1 & 0 \\ 0 & 0 & 1 \end{bmatrix}, \text{ and } \boldsymbol{A}_{1h} = \begin{bmatrix} 1 & 0 & 0 \\ 0 & 0 & 0 \\ 0 & 0 & 0 \end{bmatrix}$$

The final state space equation is

$$\begin{cases} \begin{bmatrix} \dot{\boldsymbol{x}}_1 \\ \dot{\boldsymbol{x}}_e \end{bmatrix} = \begin{bmatrix} \boldsymbol{A}_1 & \boldsymbol{0} \\ \boldsymbol{B}_e & \boldsymbol{A}_e \end{bmatrix} \begin{bmatrix} \boldsymbol{x}_1 \\ \boldsymbol{x}_e \end{bmatrix} + \begin{bmatrix} \boldsymbol{B}_1 \\ \boldsymbol{0} \end{bmatrix} \boldsymbol{T}_c + \begin{bmatrix} \boldsymbol{B}_w \\ \boldsymbol{0} \end{bmatrix} \boldsymbol{w} \\ \boldsymbol{T}_c = -\begin{bmatrix} \boldsymbol{K}_1 & \boldsymbol{K}_e \end{bmatrix} \begin{bmatrix} \boldsymbol{x}_1 \\ \boldsymbol{x}_e \end{bmatrix} \end{cases} \tag{52}$$

This is a 30-dimensional state space equation. To facilitate the solution of the feedback gain matrix, an improved linear quadratic regulator with an eigenvalue placement algorithm will be introduced in part C.

C. LINEAR QUADRATIC REGULATOR WITH EIGENVALUE PLACEMENT

Consider the linear time-invariant controllable system described by

$$\dot{\boldsymbol{x}} = \boldsymbol{A}\boldsymbol{x} + \boldsymbol{B}\boldsymbol{u}; \quad \boldsymbol{x}(0) = \boldsymbol{0} \tag{53}$$

where $\boldsymbol{x}$ is the state vector, $\boldsymbol{u}$ is the input vector, and $\boldsymbol{A}$ and $\boldsymbol{B}$ are constant matrices of appropriate dimensions. Let the quadratic cost function for (53) be

$$\boldsymbol{J} = \int_0^\infty \left[\boldsymbol{x}^T \boldsymbol{Q} \boldsymbol{x} + \boldsymbol{u}^T \boldsymbol{R} \boldsymbol{u} \right] dt \tag{54}$$

where $\boldsymbol{Q}$ and $\boldsymbol{R}$ are non-negative and positive weight matrices. The feedback controller that minimizes the cost function can be expressed as (55) by solving the matrix Riccati equation (56):

$$\boldsymbol{u} = -\boldsymbol{R}\boldsymbol{B}^T \boldsymbol{P} \boldsymbol{x} \triangleq -\boldsymbol{K}\boldsymbol{x} \tag{55}$$

$$\boldsymbol{P}\boldsymbol{B}\boldsymbol{R}^{-1}\boldsymbol{B}^T\boldsymbol{P} - \boldsymbol{A}^T\boldsymbol{P} - \boldsymbol{P}\boldsymbol{A} - \boldsymbol{Q} = \boldsymbol{0} \tag{56}$$

In order to avoid the selection of weight matrix $\boldsymbol{Q}$ and make the system have better dynamic characteristics, we use the pole placement algorithm introduced by Shieh *et al.* [24]. This technology can place the close-loop poles in a sector region with a sector angle $\pm\pi/2k$, $k = 2, 3$ from the negative real axis in the s-plane the and left hand of the $-h$ vertical line (Fig. 4), where $h \geq 0$ represents the prescribed degree of relative stability. This algorithm places closed-loop poles within the open sector using numerical iteration.

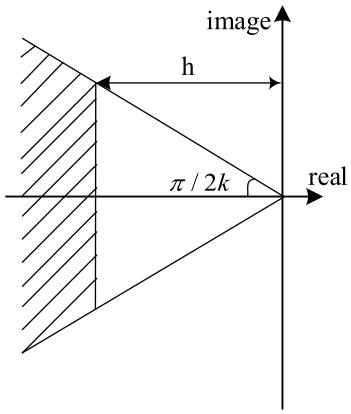

FIGURE 4. Specified region for pole placement.

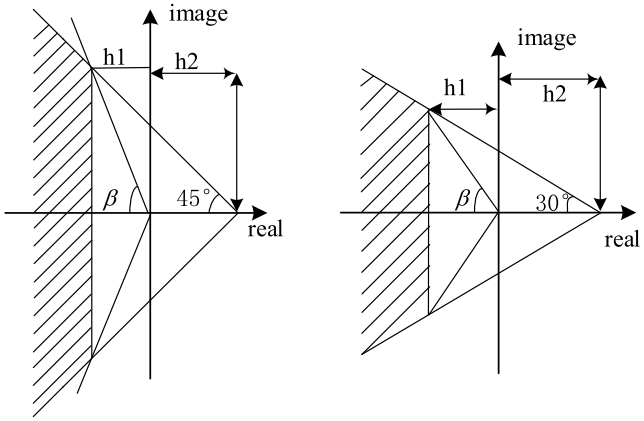

FIGURE 5. Shift region for pole placement.

The best dynamic property of the control system will be obtained when the closed –loop poles are placed near $\pm\pi/2$, but the largest region that can be considered is bounded by lines of $\pm\pi/4$. To better achieve the dynamic property of control system and increase the flexibility of the pole placements, a shifted sector method is proposed in Fig. 5, whereby the poles can be placed at any sector angle β between 30° and 90°. The design steps are as follows.

Step 1) Given a linear system as in (53), assign h such that $-h$ is parallel with the imaginary axis, which would represent the line beyond which the closed-loop pole will be placed in the sector shown in Fig. 4. Assign the positive-definite matrix $\boldsymbol{R}$, and solve the equation

$$\boldsymbol{P}_0\boldsymbol{B}\boldsymbol{R}^{-1}\boldsymbol{B}^{\mathrm{T}}\boldsymbol{P}_0 - \boldsymbol{P}_0(\boldsymbol{A} + h\boldsymbol{E}_n) - (\boldsymbol{A} + h\boldsymbol{E}_n)^T\boldsymbol{P}_0 = 0 \quad (57)$$

Solve the symmetric positive semi-definite matrix $\boldsymbol{P}_0$. The immediate closed-loop system matrix is $\boldsymbol{A}_1 = \boldsymbol{A} - \boldsymbol{B}\boldsymbol{R}^{-1}\boldsymbol{B}^T\boldsymbol{P}_0$, and hence all the poles are in the left-hand plane beyond the $-h$ vertical line. Set $i = 1$.

Step 2) Assign an angle β for the sector, and $h_1 = h$ in Fig. 5. If $\beta \in (30°, 45°)$ go to Step3); otherwise $\beta \in (45°, 90°)$ and proceed to Step7). Step 3) For assignment angle β, move the imaginary axis to the right:

$$h2 = \sqrt{3}h_1 \tan\beta - h_1 \quad (58)$$

Obtain the new state matrix $\boldsymbol{A}_1 = \boldsymbol{A}_1 - \boldsymbol{E}h_2$;

Step 4). Solve the equation

$$\hat{\boldsymbol{Q}}_i\boldsymbol{B}\boldsymbol{R}^{-1}\boldsymbol{B}^T\hat{\boldsymbol{Q}}_i - \hat{\boldsymbol{Q}}_i(\boldsymbol{A}_1^3) - (\boldsymbol{A}_1^3)^T\hat{\boldsymbol{Q}}_i - 0 = 0 \quad (59)$$

Obtain the symmetric positive semi-definite solution matrix $\hat{\boldsymbol{Q}}_i$. Check if $0.5tr(\boldsymbol{B}\boldsymbol{R}^{-1}\boldsymbol{B}^T\hat{\boldsymbol{Q}}_i) = 0$; if so, proceed to V, but otherwise continue.

Step 5) Solve the equation

$$\boldsymbol{P}_i\boldsymbol{B}\boldsymbol{R}^{-1}\boldsymbol{B}^{\mathrm{T}}\boldsymbol{P}_i - \boldsymbol{P}(\boldsymbol{A}_i) - \boldsymbol{A}_i^T\boldsymbol{P} - \hat{\boldsymbol{Q}}_i = 0 \quad (60)$$

Obtain solution $\boldsymbol{P}_i$; the immediate closed-loop system matrix is therefore $\tilde{\boldsymbol{A}} = \boldsymbol{A}_i - \gamma_i\boldsymbol{B}\boldsymbol{R}^{-1}\boldsymbol{B}^T\boldsymbol{P}_i$. Solve for the coefficient γ_i from the inequality

$$a_1\gamma_i^3 + b_1\gamma_i^2 + c_1\gamma_i + d_1 \le 0 \quad (61)$$

where $a_1 = -\mathrm{tr}[(\boldsymbol{B}\boldsymbol{R}^{-1}\boldsymbol{B}^T\boldsymbol{P}_i)^3]$, $b_1 = 3\mathrm{tr}(\boldsymbol{B}\boldsymbol{R}^{-1}\boldsymbol{B}^T\boldsymbol{P}_i)^2\boldsymbol{A}_i$, $c_1 = -3\mathrm{tr}(\boldsymbol{B}\boldsymbol{R}^{-1}\boldsymbol{B}^T\boldsymbol{P}_i)\boldsymbol{A}_i^2$, and $d_1 = 0.5\mathrm{tr}(\boldsymbol{B}\boldsymbol{R}^{-1}\boldsymbol{B}^T\hat{\boldsymbol{Q}}_i)$.

Step 6) Set $i = i + 1$ and proceed to Step4)

Step 7) For the assignment angle β, move the imaginary axis to the right:

$$h2 = h_1 \tan\beta - h_1 \quad (62)$$

Obtain the new state matrix $\boldsymbol{A}_1 = \boldsymbol{A}_1 - \boldsymbol{E}h_2$.

Step 8) Solve the equation

$$\hat{\boldsymbol{Q}}_i\boldsymbol{B}\boldsymbol{R}^{-1}\boldsymbol{B}^T\hat{\boldsymbol{Q}}_i - \hat{\boldsymbol{Q}}_i(-\boldsymbol{A}_i^2) - (-\boldsymbol{A}_i^2)^{\mathrm{T}}\hat{\boldsymbol{Q}}_i - 0 = 0 \quad (63)$$

Obtain the solution of the symmetric positive semi definite matrix $\hat{\boldsymbol{Q}}_i$. Check if $0.5tr(\boldsymbol{B}\boldsymbol{R}^{-1}\boldsymbol{B}^T\hat{\boldsymbol{Q}}_i) = 0$. If so, proceed to V, but otherwise continue.

Step 9) Solve the equation

$$\boldsymbol{P}_i\boldsymbol{B}\boldsymbol{R}^{-1}\boldsymbol{B}^T\boldsymbol{P}_i - \boldsymbol{P}\boldsymbol{A}_i - \boldsymbol{A}_i^T\boldsymbol{P} - \hat{\boldsymbol{Q}}_i = 0 \quad (64)$$

Obtain the solution $\boldsymbol{P}_i$; the immediate closed-loop system matrix is therefore $\tilde{\boldsymbol{A}} = A_i - \gamma_i\boldsymbol{B}\boldsymbol{R}^{-1}\boldsymbol{B}^T\boldsymbol{P}_i$. Solve for the coefficient γ_i:

$$\gamma_i = \max\{0.5, \frac{b_2 + \sqrt{(b_2^2 + a_2c_2}}{a_2}\} \quad (65)$$

where $a_2 = -\mathrm{tr}[(\boldsymbol{B}\boldsymbol{R}^{-1}\boldsymbol{B}^T\boldsymbol{P}_i)^2]$, $b_2 = \mathrm{tr}(\boldsymbol{B}\boldsymbol{R}^{-1}\boldsymbol{B}^T\boldsymbol{P}_i)\boldsymbol{A}_i$, and $c_2 = 0.5tr(\boldsymbol{B}\boldsymbol{R}^{-1}\boldsymbol{B}^T\hat{\boldsymbol{Q}}_i)$.

Step 10) Set $i = i + 1$ and proceed to Step8).

Step 11) The algorithm is completed, all of the closed-loop system poles are in the specified region of Fig. 5, and the optimal feedback is

$$\boldsymbol{K} = \boldsymbol{B}\boldsymbol{R}^{-1}\boldsymbol{B}^T(\boldsymbol{P}_0 + \gamma_1\boldsymbol{P}_1 + \cdots + \gamma_j\boldsymbol{P}_j) \quad (66)$$

Finally, the optimal regulator can be given as $\boldsymbol{u} = -\boldsymbol{K}\boldsymbol{x}$.

NOTE 2: This pole placement technology, which is utilized to compute CAMF and the attitude manoeuvre controller, has an advantage over the traditional LQR algorithm; the feedback matrices can be obtained by setting the performance indexes without choosing a weight matrix Q, which is efficient and easy for high-dimension space state equations. The gain matrix designed by this algorithm is more convenient than the reference [15].

V. NUMERICAL EXAMPLE

The multistage attitude control strategy proposed in this paper was verified through mathematical simulation. To obtain accurate gravitational gradients and aerodynamic moments, we established the orbital model. The orbital elements included the semimajor axis (a_s), eccentricity (e), right ascension of the ascending node (Ω), orbital inclination (I), argument of perigee (ω), and true anomaly ($\theta(t_0)$), the values of which are shown in table 1. The atmospheric density ρ in (7) is influenced by many factors, including seasonal effects, solar activity, the day/night cycle, orbital geometry and the earth's magnetic activity. We utilized NRLMSISE-00 [25] to obtain real-time atmospheric densities. Fig. 6 shows the structure of the space station. We can therefore calculate the aerodynamic torques according to (7), which is more accurate than other algorithms.

TABLE 1. Orbital elements.

a_s	e	Ω	I	ω	$\theta(t_0)$
6779.1Km	0.0001	90°	40°	45°	0°

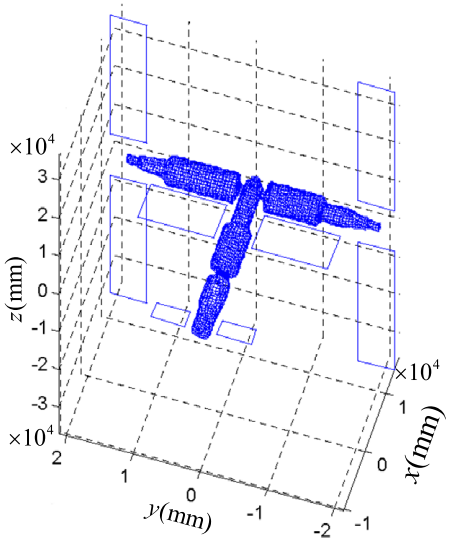

FIGURE 6. S Space station structure.

Considering that there is not a singularity problem arising from the variable speed control moment gyros (VSCMGs), two clusters of VSCMGs in a pyramid configuration were utilized as the control actuators [26], and each of the VSCMGs had a nominal angular momentum of 2000 $N.ms$. In this case, we assumed that a cargo spaceship docks with the core module in the radial direction (Fig. 6). The following inertia matrix was specified for the space station:

$$\boldsymbol{I}^b = \begin{bmatrix} 55.94 & -0.2201 & 0.1854 \\ -0.2201 & 64.27 & 0.3125 \\ 0.1854 & 0.3125 & 107.6 \end{bmatrix} \times 10^5 \text{ kg.m}^2.$$

For the TEA tracking, the feedback matrix $\boldsymbol{K}_2$ in (49) was chosen by the LQR with the eigenvalue placement algorithm. The related performance indexes were assigned as $\boldsymbol{R} = \boldsymbol{E}$, $h = 0.01$, and $\beta = 60°$. An interesting phenomenon is that all of the system poles were configured to -0.02. The initial attitude was $\boldsymbol{\theta} = \begin{bmatrix} 0.4° & 0.5° & -0.3° \end{bmatrix}^{\mathrm{T}}$, and the initial angular velocity was chosen as $\boldsymbol{\omega}_b = \begin{bmatrix} 0 & 0 & 0 \end{bmatrix}^T$ rad/s. Using curve fitting, we isolated the constant and cyclic components at the orbital rate of the disturbance and expressed the components in the orbital frame as

$$\boldsymbol{T}_d^o = \begin{bmatrix} -0.017 \\ -0.97 \\ 0.012 \end{bmatrix} + \begin{bmatrix} -0.036\sin(\omega_o t) + 0.049\cos(\omega_o t) \\ 0.086\sin(\omega_o t + 3\pi/4) \\ -0.15\sin(\omega_o t) + 0.095\cos(\omega_o t) \end{bmatrix} \text{(N.m)}. \tag{67}$$

We set the adjusting time as $t_{s1} = t_{s3} = 500s$. Four orbital periods were utilized to unload the VSCMGs angular momentum. According to the dynamic characteristics of TEA tracking, the coefficient in (37) was $\vartheta_1 = 0.07156$. Hence the coefficients in (36) could be obtained easily. Similarly, we set $\alpha \approx \pi 7/6$ in (30) according to (66), and the k_x in (40) was estimated as $k_x = 0.00912$; the coefficients of attitude path of roll angle in (38) could therefore also be obtained.

It is easily shown that the inertia matrix meets the constraint condition in (35), which means the CAMF system is controllable. The parameters in (52) are shown in table 2. The CAMF controller gain was computed using the linear quadratic regulator with the eigenvalue placement algorithm. To obtain good dynamic performance, the pole placement related parameters were assigned to $\boldsymbol{R} = \boldsymbol{E}_3$, $h = 0.4\omega_o$, and $\beta = 60°$. All of the closed-loop poles were placed to the left of the line at $0.4\omega_o$ and within a sector angle of 60° (Fig. 7). Hence the system possessed proper transient response and robustness properties.

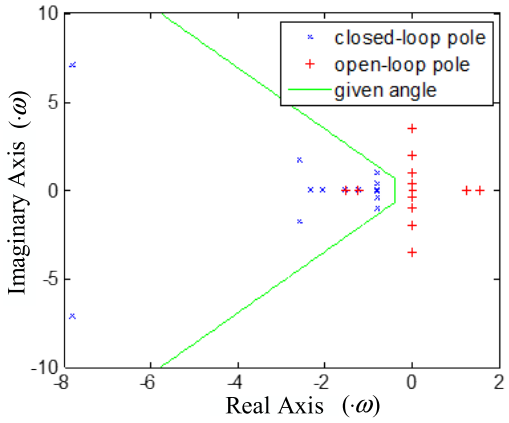

FIGURE 7. System poles of CAMF.

The numerical results are presented in Fig. 8 to Fig. 13. This simulation can be divided into three parts: attitude stabilization, TEA tracking and CAMF. Attitude stabilization lasted for approximately two orbital periods (185 minutes) for rendezvous and docking (Fig. 8). Before the attitude control strategy switched from attitude stabilization to CAMF,

TABLE 2. CAMF parameters.

t_x	t_y	t_z	λ_1	λ_2
0.043	1.1	0.21	2	3.5

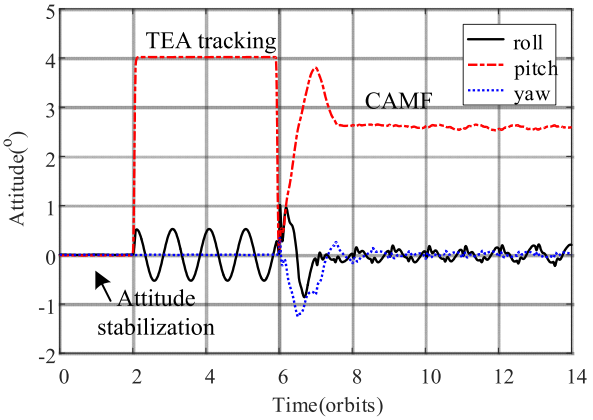

FIGURE 8. Space station attitude.

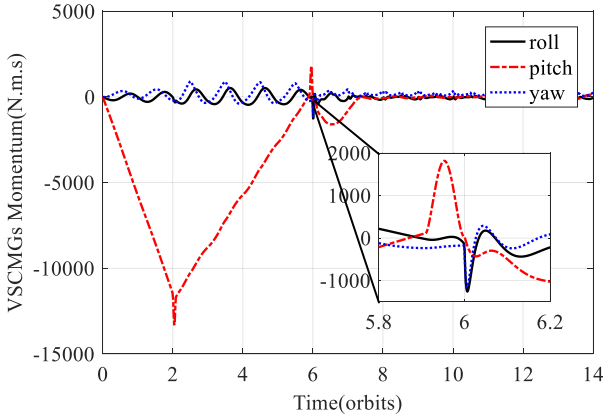

FIGURE 9. VSCMGs angular momentum.

the VSCMGs should be unloaded because a large amount of momentum would accumulate in the attitude stabilization mode (Fig. 9). Otherwise, the model error between the real system and the linearized system would be amplified, which would cause the system to become unstable and shake.

The VSCMGs momentum was unloaded in four orbit periods before the space station flew in CAMF mode over the next eight orbital periods (Fig. 8 and Fig. 9). The attitude-related gravity term and the aerodynamic torques (Fig. 10 and Fig. 12,) were utilized to unload the VSCMGs momentum (Fig. 9) and offset the disturbance at the same time during the attitude manoeuvre. The VSCMGs momentum was within $\pm 500 N.m.s$ at the shift point (Fig. 9). The attitude control switched from the TEA tracking mode to the CAMF mode smoothly over six orbital periods (Fig. 8).

During the CAMF stage, the pitch angle was approximately 3.3°, the roll angle underwent sinusoidal motion at the orbital frequency, and the yaw angle remained at zero (Fig. 8), which means the perturbation on the yaw axis was absorbed by the rolling axis movement. By combining Fig. 9,

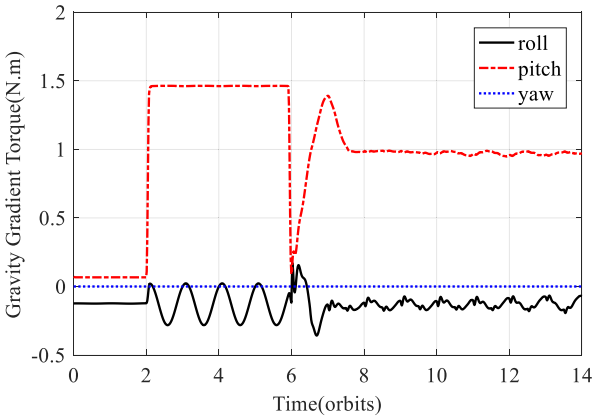

FIGURE 10. Gravity gradient torque.

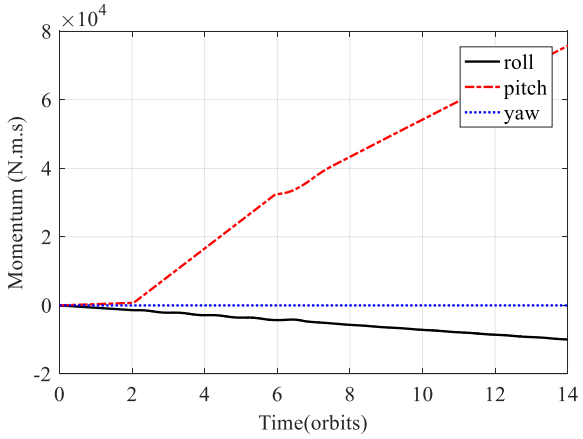

FIGURE 11. Angular momentum accumulation caused by gravity gradient torques.

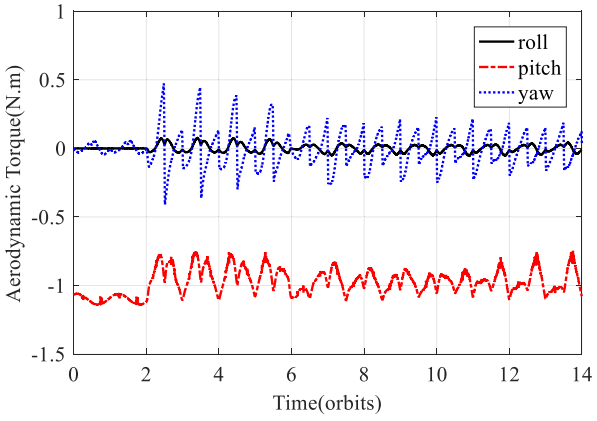

FIGURE 12. Aerodynamic torques.

Fig. 11 and Fig. 13, it can be seen that the accumulation of angular momentum caused by the constant disturbance was perfectly absorbed by the gravity gradient and aerodynamic torques through the attitude manoeuvre. Although the disturbances with frequencies ω_o, $2\omega_o$, and $3.5\omega_o$ were suppressed by the controller, the high-order attitude perturbation remained (Fig. 8) because it was difficult to estimate the high-order disturbance (Fig. 12). However, the controller that accounted for the disturbance suppression performed

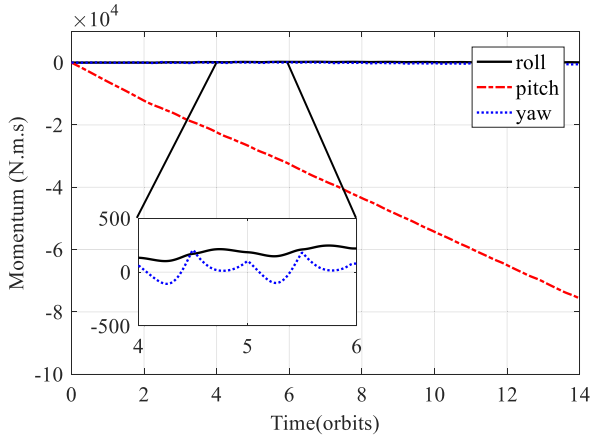

FIGURE 13. Angular momentum accumulation caused by aerodynamic torques.

better than its counterpart that did not account for disturbance suppression.

VI. CONCLUSIONS

A multistage attitude control algorithm for space stations using VSCMGs was proposed in this paper. To ensure that the VSCMGs angular momentum is unloaded before the control mode is switched from attitude stabilization to CAMF, a TEA tracking controller was designed. TEA tracking, which is realized using an attitude manoeuvre, is an open-loop control strategy, which means that its control effect depends on the system model. Obviously, it is difficult to obtain an accurate system model, and as a consequence, the VSCMGs angular momentum cannot be unloaded to zero at the end of the attitude manoeuvre. Fortunately, holding the VSCMGs angular momentum over a small range is sufficient to avoid the shocking of attitude at the initial moment, and the method still has significant practical value. Based on a three-axis coupled linearized model, a CAMF controller based on the LQR method and the internal model principle was proposed to achieve ACMM. Because of the disturbance model introduced in the system, the influences of environmental torques on attitude are well suppressed. The pole placement algorithm yields a good solution to the problem of choosing the proper weight matrix, especially for multidimensional matrices. In this case, no jet propulsion is needed during the entire process.

REFERENCES

[1] Y. Kimoto, K. Yano, J. Ishizawa, E. Miyazaki, and I. Yamagata, "Passive space-environment-effect measurement on the international space station," *J. Spacecraft Rockets*, vol. 46, no. 1, pp. 22–27, 2009, doi: 10.2514/1.31851.

[2] K. A. Ford and C. D. Hall, "Singular direction avoidance steering for control-moment gyros," *J. Guid., Control, Dyn.*, vol. 23, no. 4, pp. 648–656, 2000, doi: 10.2514/2.4610.

[3] E. Messerschimd, *Space Stations: Systems and Utilization*. New York, NY, USA: Springer, 1999, chs. 6–8.

[4] M. Zhu and S. Xu, "Stability-based SDRE controller for spacecraft momentum management," *Acta Astronsutica*, vol. 89, no. 1, pp. 71–82, 2013. [Online]. Available: https://doi.org/10.1016/j.actaastro.2013.03.026

[5] V. A. Sarychev, V. P. Legostaev, V. V. Sazonov, M. Y. Belyaev, I. N. Gansvind, and T. N. Tyan, "The passive attitude motion of the orbital stations Salyut-6 and Salyut-7," *Acta Astronsutica*, vol. 15, no. 9, pp. 635–640, 1987, doi: 10.1016/0094-5765(87)90134-2.

[6] P. D. Hatis, "Predictive Momentum management for the space station," *J. Guid., Control Dyn.*, vol. 9, no. 4, pp. 454–461, 1985, doi: 10.2514/3.20132.

[7] R. Kumar, M. Heck, and B. Robertson, "Predicted torque equilibrium attitude utilization for space station attitude control," in *Proc. AIAA Guid., Navigat., Control Conf.*, Washington, DC, USA, Aug. 1990, pp. 29–41, paper AIAA-90-3318, doi: 10.2514/6.1990-3318.

[8] V. A. Sarychev, A. Guerman, and P. Paglione, "Influence of constant torque on equilibria of satellite in circular Orbit," *Celestial Mech. Dyn. Astron.*, vol. 87, no. 3, pp. 219–239, 2003, doi: 10.1023/B:CELE.0000005713.66553.88.

[9] V. A. Sarychev, S. A. Mirer, A. A. Degtyarev, and E. K. Duarte, "Investigation of equilibria of a satellite subjected to gravitational and aerodynamic torques," *Celestial Mech. Dyn. Astron.*, vol. 97, no. 4, pp. 267–287, 2007, doi: 10.1007/s10569-006-9064-3.

[10] V. A. Sarychev, S. A. Mirer, and A. A. Degtyarev, "Equilibria of a satellite subjected to gravitational and aerodynamic torques with pressure center in a principal plane of inertia," *Celestial Mech. Dyn. Astron.*, vol. 100, no. 4, pp. 301–318, 2008, doi: 10.1007/s10569-008-9126-9.

[11] E. Shain and V. Spector, "Adaptive torque equilibrium control of the space station," in *Proc. AIAA 23rd Aerosp. Sci. Meeting*, Reno, NV, USA, pp. 301–318, paper AIAA-85-0028, 1985, doi: /10.2514/6.1985-28.

[12] B. Wie, K. W. Byun, V. W. Warren, D. Geller, D. Long, and J. Sunkel, "New approach to attitude/momentum control for the Space Station," *J. Guid., Control, Dyn.*, vol. 12, no. 5, pp. 714–722, 1989, doi: 10.2514/3.20466.

[13] W. Warren, B. Wie, and D. Geller, "Periodic-disturbance accommodating control of the Space Station for asymptotic momentum management," *J. Guid., Control, Dyn.*, vol. 13, no. 6, pp. 984–992, 1990, doi: 10.2514/3.20570.

[14] J. W. Sunkel and L. S. Shieh, "Multistage design of an optimal momentum management controller for the Space Station," *J. Guid., Control, Dyn*, vol. 14, no. 3, pp. 492–502, 1991, doi: 10.2514/3.20668.

[15] J. T. Harduvel, "Continuous momentum management of earth-oriented spacecraft," *J. Guid., Control, Dyn.*, vol. 15, no. 6, pp. 1417–1426, 1992, doi: 10.2514/3.11405.

[16] M. Xin and S. N. Balakrishnan, "A new method for suboptimal control of a class of non-linear systems," *Optim. Control Appl. Methods*, vol. 26, no. 2, pp. 55–83, 2005, doi: 10.1002/oca.750.

[17] I. V. Sorokin and A. V. Markov, "Utilization of space stations: 1971–2006," *J. Spacecraft Rockets*, vol. 45, no. 3, pp. 600–607, 2008, doi: 10.2514/1.32772.

[18] G. E. Funk and R. M. Stephenson, "On-orbit shuttle/Mir mated reaction control system and crew load analyses," *J. Spacecraft Rockets*, vol. 37, no. 4, pp. 515–518, 2000. [Online]. Available: https://doi.org/10.2514/2.3593

[19] K. Jules, K. McPherson, K. Hrovat, E. Kelly, and T. Reckart, "A status report on the characterization of the microgravity environment of the International Space Station," *Acta Astronsutica*, vol. 55, nos. 3–9, pp. 335–364, 2004, doi: 10.1016/j.actaastro.2004.05.057.

[20] D. J. Newman, A. R. Amir, and S. M. Beck, "Astronaut-induced disturbances to the microgravity environment of the Mir Space Station," *J. Spacecraft Rockets*, vol. 38, no. 4, pp. 578–583, 2001, doi: 10.2514/2.3719.

[21] B. A. Francis and W. M. Wonham, "The internal model principle of control theory," *Automatica*, vol. 12, no. 5, pp. 457–465, 1976, doi: 10.1016/.0005-1098(76)90006-6.

[22] B. A. Francis and W. M. Wonham, "The internal model principle for linear multivariable regulators," *Appl. Math. Optim.*, vol. 2, no. 2, pp. 170–194, 1975, doi: 10.1007/BF01447855.

[23] D. Z. Zheng, *Linear Systems Theory*, 2nd ed. Beijing, China: Tsinghua Univ. Press, 2005, ch. 4.

[24] L. S. Shieh, H. M. Dib, and G. Sekar, "Continuous-time quadratic regulators and pseudo-continuous-time quadratic regulators with pole placement in a specific region," *IEE Proc., Control Theory Appl.*, vol. 134, no. 5, pp. 338–346, 1987, doi: 10.1049/.ip-d:19870056.

[25] J. M. Picone, A. E. Hedin, D. P. Drob, and A. C. Aikin, "NRLMSISE-00 empirical model of the atmosphere: Statistical comparisons and scientific issues," *J. Geophys. Res.*, vol. 107, no. A12, pp. 1–16, 2002, doi: 10.1029/2002JA0.09430.

[26] X. Huang, Y. Jia, S. Xu, and T. Huang, "A new steering approach for VSCMGs with high precision," *Chin. J. Aeronautics*, vol. 29, no. 6, pp. 1673–1684, 2016, doi: 10.1016/j.cja.2016.10.017.

QINGQING DANG received the B.S. degree from Liaoning Technical University, China. He is currently pursuing the Ph.D. degree with the School of Astronautics, Beihang University. His research interests include dynamics and control of spacecraft.

LEI JIN received the Ph. D. degree from Beihang University, China. She is currently an Associate Professor with the Department of GNC for Aerospace, School of Astronautics, Beihang University. Her current research interests include dynamics and control of spacecraft.